LIQUID CRYSTALS, 2001, VOL. 28, NO. 9, 1389–1402

Backflow-affected relaxation in nematic liquid crystals

D. SVENŠEK* and S. ŽUMER

Oddelek za fiziko, Univerza v Ljubljani, Jadranska 19, 1000 Ljubljana, Slovenija

(*Received 23 October 2000; accepted 16 April 2001*)

A complete numerical study of a two-dimensional nematic backflow problem is presented. Nematodynamic equations are reviewed, and characteristic scales are introduced. The relaxation under the application and suppression of a magnetic field is studied in square- and rectangular-shaped cells. Solutions for the flow fields, director fields, and director time derivative fields are given and these are interpreted to gain a qualitative understanding of the problem. The backflow is found to depend critically on the geometry of the cell. The complete solution is compared with the simplified approach in which the backflow is neglected. The discrepancy depends strongly on the cell geometry.

1. Introduction

Problems involving hydrodynamic motion of a nematic liquid crystal due to director reorientation have been studied mainly in terms of the Ericksen–Leslie continuum theory of the nematic liquid crystal [1, 2]. For one-dimensional geometry, Clark and Leslie [3] have given a thorough approximative analysis of nematic relaxation upon the removal of an electric or magnetic field; a complete numerical treatment of the problem has been given by van Doorn [4]. Pieranski, Brochard and Guyon [5, 6] have studied, both theoretically and experimentally, the one-dimensional dynamic behaviour in a magnetic field for three geometries (twisted, planar to homeotropic, homeotropic to planar), limited to small deformations (applying near-critical fields). They give the distortion wave vector and effective viscosity dependence on the magnetic field strength. The instability against periodic distortion in the case of the Freedericksz transition (first observed by Carr [7]) has been studied by Guyon *et al.* [8] for the two-dimensional case, and by Hurd *et al.* [9] for three dimensions. The pattern formation in a rotating magnetic field has been observed experimentally and accounted for by a numerical study based on the Ericksen–Leslie equations [10, 11]. An experiment measuring the rotational viscosity is described by Bajc [12], together with a full hydrodynamic numerical treatment in a cylindrical geometry (one dimension), yielding an exact expression for the effective viscosity, depending on the director field configuration and thus on time. Recently, a two-dimensional hydrodynamic description of a rotating nematic sample in a magnetic field was published [13], neglecting the backflow; however, since the flow field was prescribed to be that of a homogeneously revolving cylinder, this simplified the problem enormously.

In this paper a full two-dimensional hydrodynamic study of a flow-aligning nematic sample in a magnetic field is presented, producing non-trivial backflow fields even in the simplest geometries such as a square or a rectangle. First a short review of nematodynamic equations is given, followed by an introduction to the characteristic scales of the problem. In the second part, the flow fields are tentatively interpreted by strict analytical as well as by less strict arguments. Also, the influence of the backflow on the director reorientation is discussed. The idea pursued throughout the paper is to provide a sufficient, qualitative physical understanding of the backflow generation and its effect on the director field, to be able to explain or even foresee the global time path of relaxation processes. The relaxation with the backflow is then compared with the simplified case where backflow is neglected. The issues in question here are the change in the switching time of the cell caused by the backflow, and the local departure of the director orientation from the orientation in the simple case, pursued along the whole path of relaxation.

2. Equations of nematodynamics

Three basic equations are involved in the problem of nematodynamics; these are the equation of motion of the director field, the generalized Navier–Stokes equation, and the equation of continuity. For most purposes the latter is simply reduced to the equation of incompressibility, whereas the former two are relatively extensive due to the (uniaxial) anisotropy of the nematic fluid as well as to the coupling between the director reorientation and flow.

*Author for correspondence;
e-mail: daniel.svensek@fmf.uni-lj.si

Liquid Crystals ISSN 0267-8292 print/ISSN 1366-5855 online © 2001 Taylor & Francis Ltd
http://www.tandf.co.uk/journals
DOI: 10.1080/02678290110067236

The time evolution equation for the director field is a balance between generalized elastic, electromagnetic and viscous forces. In principle, both electric and magnetic fields can be used to manipulate the nematic director. However, the use of an electric field, though more efficient, brings about some difficulties to deal with, i.e. the dielectric problem has to be solved exactly, and the convection of ions should be taken into account. As a result of this, the theoretical study to be presented in this paper uses a magnetic field. To obtain the elasto-magnetic part, the Frank elastic free-energy density function [14, pp. 102, 119] is used:

$$f = \frac{1}{2}K_{11}(\nabla \cdot \mathbf{n})^2 + \frac{1}{2}K_{33}[\mathbf{n}\times(\nabla\times\mathbf{n})]^2 - \frac{1}{2}\frac{\chi_a}{\mu_0}(\mathbf{n}\cdot\mathbf{B})^2 \tag{1}$$

where $\mathbf{n}$ is a unit vector representing the director, K_{11} and K_{33} are the splay and the bend elastic constants, respectively, $\mathbf{B}$ is the magnetic field, and χ_a is the magnetic susceptibility anisotropy, i.e. the difference between the susceptibilities parallel and perpendicular to the director. The case of $\chi_a > 0$ will be considered here, as this is the situation present in most nematic substances. According to the limitation of two-dimensional problems, the twist term is missing in equation (1); furthermore, the surface terms have been dropped in (1) on account of fixed boundary conditions. Parametrizing $\mathbf{n} = (\cos\varphi, \sin\varphi)$, the Euler–Lagrange equation for the function (1) gives the elasto-magnetic generalized force:

$$h^{em} = -\frac{\partial f}{\partial\varphi} + \partial_i\left[\frac{\partial f}{\partial(\partial_i\varphi)}\right]. \tag{2}$$

The viscous generalized force is obtained from the dissipation function containing scalar invariants formed with $\mathbf{n}$, $\dot{\mathbf{n}}$ and $\nabla\mathbf{v}$ [15, p. 142]:

$$\mathbf{h}^v = -\gamma_1\mathbf{N} - \gamma_2 \mathrm{A}\cdot\mathbf{n} \tag{3}$$

where the rotational viscosity γ_1 and γ_2 are expressed in terms of the Leslie viscosity coefficients α_i, $\gamma_1 = \alpha_3 - \alpha_2$, $\gamma_2 = \alpha_3 + \alpha_2$. With $\dot{\mathbf{n}}$ being the material time derivative of the director,

$$\mathbf{N} = \dot{\mathbf{n}} - \frac{1}{2}(\nabla\times\mathbf{v})\times\mathbf{n} = \dot{\mathbf{n}} + \mathrm{W}\cdot\mathbf{n}$$

is the vector of the relative director rotation with respect to the rotation of the fluid, and finally

$$\mathrm{A}_{ij} = \frac{1}{2}(\partial_i v_j + \partial_j v_i)$$

$$\mathrm{W}_{ij} = \frac{1}{2}(\partial_i v_j - \partial_j v_i)$$

are the symmetric and antisymmetric parts of the velocity gradient, respectively. In the angle parametrization of the director, the viscous force becomes

$$h^v = (\mathbf{n}\times\mathbf{h}^v)_z. \tag{4}$$

Thus, the equation of motion of the director reads briefly as,

$$h^{em} + h^v = 0. \tag{5}$$

The generalized Navier–Stokes equation,

$$\rho\frac{\mathrm{d}\mathbf{v}}{\mathrm{d}t} = -\nabla p + \nabla\cdot(\sigma^v + \sigma^e) \tag{6}$$

where ρ is the density and p is the pressure, involves two stress tensor contributions. The viscous part is obtained from the same dissipation function as the generalized force (3) [15, p. 142]:

$$\sigma^v = \alpha_1\mathbf{n}\otimes\mathbf{n}(\mathbf{n}\cdot\mathrm{A}\cdot\mathbf{n}) + \alpha_2\mathbf{n}\otimes\mathbf{N} + \alpha_3\mathbf{N}\otimes\mathbf{n} + \alpha_4\mathrm{A} + \alpha_5\mathbf{n}\otimes(\mathrm{A}\cdot\mathbf{n}) + \alpha_6(\mathrm{A}\cdot\mathbf{n})\otimes\mathbf{n} \tag{7}$$

where α_i terms are the Leslie viscosity coefficients. The elastic part of the stress tensor is a consequence of deformations changing the director field gradients, [14, p. 152]:

$$\sigma^e_{ij} = -\frac{\partial f}{\partial(\partial_i n_k)}\partial_j n_k. \tag{8}$$

The pressure field in equation (6) is set by the incompressibility condition

$$\nabla\cdot\mathbf{v} = 0 \tag{9}$$

i.e. it has to be determined in such a way that the flow be incompressible.

2.1. *Characteristic scales*

In this section the equations will be rewritten in a dimensionless form, introducing the characteristic time and length scales of the problem. Lengths are to be measured in terms of the container size L:

$$x \to \frac{x}{L}.$$

Another characteristic length, the magnetic coherence length $\xi_m = (\mu_0 K_{11}/|\chi_a|B^2)^{1/2}$ will serve as a measure for the magnetic field strength:

$$B \to \frac{B}{B_0}$$

where B_0 is the magnetic field strength giving a coherence length of L. The time scale of the problem is determined by the typical relaxation time of the director field

deformed over the distance L,

$$t \to \frac{t}{\tau}, \quad \tau = \frac{\gamma_1 L^2}{K_{11}} \tag{10}$$

which is of the order of 1 s for a 10 μm sample. Typical relaxation time in a magnetic field is τ/B^2, where B is the field strength in the dimensionless units introduced earlier. Another time scale is given by a typical transition time during which the velocity field equilibrates due to viscous and elastic forces,

$$\tau_0 = \frac{\rho L^2}{\gamma_1}. \tag{11}$$

The ratio τ_0/τ is very small, typically of the order 10^{-6}. The remaining quantities are expressed in terms of these units, thus:

$$v \to \frac{v}{L/\tau}, \qquad p \to p\frac{\tau^2}{\rho L^2}$$

$$K_{ii} \to \frac{K_{ii}}{K_{11}}, \quad \alpha_i \to \frac{\alpha_i}{\gamma_1}.$$

Equations (5) and (6) now read as

$$\frac{\partial \varphi}{\partial t} + (\mathbf{v} \quad \nabla)\varphi = h^{\mathrm{em}} - (\alpha_3 + \alpha_2)(\mathbf{n} \times (A \quad \mathbf{n}))_z + \frac{1}{2}(\nabla \times \mathbf{v})_z \tag{12}$$

$$\frac{\partial \mathbf{v}}{\partial t} + (\mathbf{v} \quad \nabla)\mathbf{v} = -\nabla p + \frac{\tau}{\tau_0}\nabla \quad (\sigma^{\mathrm{v}} + \sigma^{\mathrm{e}}). \tag{13}$$

Equation (13) can be simplified further by noting that the Reynolds number, $Re = \tau_0/\tau$, is very small, and hence the second left-hand side term can be omitted. Additionally, due to the big difference in the relaxation times τ and τ_0, the velocity field adapts almost instantaneously to a given director field and its time derivative. Therefore the velocity field can be solved for its final value while keeping the director field fixed, yielding

$$0 = -\nabla p + \frac{\tau}{\tau_0}\nabla \quad (\sigma^{\mathrm{v}} + \sigma^{\mathrm{e}}). \tag{14}$$

3. Description of the problem and a numerical implementation

In this paper the relaxation of a nematic sample upon turning on and switching off a magnetic field is studied. The problem considered is two-dimensional (figure 1): the quantities involved depend on x and y, while the director is lying in the xy plane. The orienting magnetic field points along the y axis. A container of square or rectangular cross section is adopted, extending to infinity in the z direction. The limit of infinitely strong anchoring is considered, which fixes the director field at the boundaries. In practice, this means that the extrapolation length [14, p. 113], ξ, must be much smaller compared both with the sample size and the magnetic coherence length, i.e. $\xi \ll L$ and $\xi \ll \xi_{\mathrm{m}}$. To avoid any frustration, the alignment is parallel for horizontal sides, while for vertical sides it is homeotropic. Standard no-slip boundary conditions are prescribed for the flow, setting the velocity to zero at the boundaries. Material parameters such as the viscosity and the elastic coefficients correspond to those for MBBA, listed in [14, pp. 105, 231].

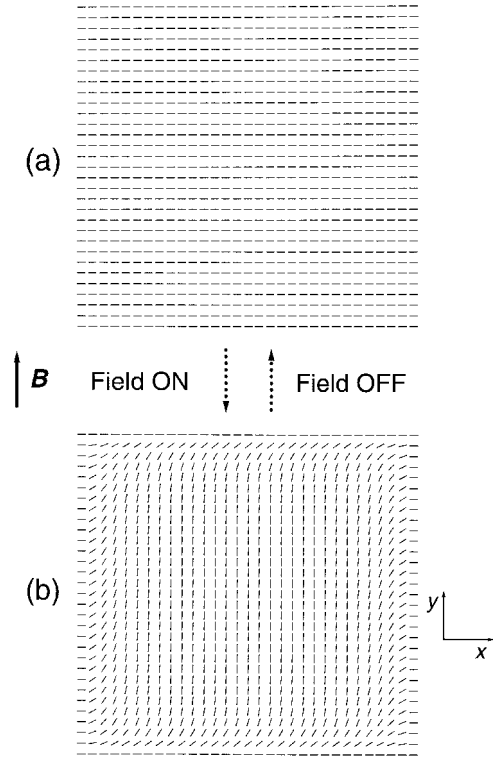

Figure 1. The calculations are performed in a square or rectangular geometry. Two types of relaxation are studied: (*a*) starting with a uniform director field, the magnetic field is switched on, or (*b*) the magnetic field is switched off to disorient a well aligned sample. The director is fixed at the boundaries as shown.

The partial differential equations (PDEs) (12) and (14) are solved using finite difference discretization. At a given director field and its time derivative, equation (14) is solved by relaxation on a staggered grid [16, p. 331], together with a Poisson equation for pressure corrections solved at every iteration step [16, p. 340]. At the boundaries, normal pressure correction derivatives are specified in order to meet the incompressibility condition. Then, knowing both the director and the velocity fields, equation (14) is advanced explicitly in time to yield the new director field. The calculations were typically done on a 40×40 grid, or larger in cases where it was necessary to observe greater detail.

4. Mechanisms governing the problem

4.1. *Backflow generation*

As indicated by calculations, the elastic stress tensor contribution (8) alters the velocity field by up to 10%. Thus, while it is of some importance when studying the flow fields, to a first approximation it can be neglected when the influence of the backflow on the director field is in question, this influence itself also being small.

Our interpretation of the velocity fields will be based solely on the viscous coupling given by equation (7). What is more, it turns out that the anisotropy of the fluid viscosity, described by terms in (7) with α_1, α_5 and α_6, has no qualitative importance. The driving force of all the interesting flow phenomena observed is the anisotropy of the coupling to the director rotation given by the two terms with α_2 and α_3 in (7). Since $\alpha_2/\alpha_3 \approx 70$, only the α_2 term needs to be taken into account when trying to interpret the results. There are two contributions to the force exerted on the fluid described by this term, one depending on the gradient of the director rotation, and the other on the director field gradient. Putting $\dot{\varphi} = \omega$ and $\varphi = 0$ one obtains

$$\mathbf{f}_1 = \alpha_2 \left(0, \frac{\partial \omega}{\partial x}\right) \tag{15}$$

for the rotation gradient dependent force. Generally, this force is always perpendicular to the director, while its magnitude depends on the ω derivative along the director, $\mathbf{n} \cdot \nabla\omega$. The second contribution is best seen if we put $\nabla\varphi = (\varphi_x, 0)$:

$$\mathbf{f}_2 = -\alpha_2 \omega \varphi_x (\cos 2\varphi, \sin 2\varphi). \tag{16}$$

Thus, the magnitude of this force depends only on $\omega|\nabla\varphi|$, whereas its direction is such that it makes twice the angle with $\nabla\varphi$ as the director. The reader should bear in mind that α_2 is negative and that the direction of the force just described depends on the sign of ω.

4.2. *Influence of backflow on the director rotation*

Let us discuss the torque on the director exerted by the flow. A flow field corresponding to a pure rotation ($\nabla \times \mathbf{v} \neq 0$, $A = 0$) imposes the same rotation on the director, as equation (12) suggests by putting $\mathbf{h}^{em}$ to zero. Conversely, pure extensional flow ($\nabla \times \mathbf{v} = 0$, $A \neq 0$) aligns the director along the axis of extension. For shear flow, which is a sum of the flows just mentioned, equation (12) gives

$$\dot{\varphi} = -\frac{1}{2}\eta \left(\frac{\gamma_2}{\gamma_1} \cos 2\varphi + 1\right) \tag{17}$$

where φ measures the angle relative to the velocity direction and η is the shear rate (see figure 2 for the sign convention). Equation (17) has a stationary solution

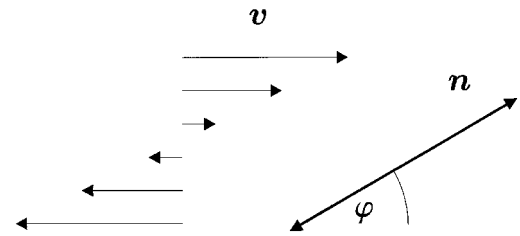

Figure 2. The director angle φ in equation (17) is measured relative to the shear as shown.

only if $|\gamma_2/\gamma_1| > 1$, i.e. if $\alpha_3 < 0$, which is the condition for the flow-aligning nematic, as opposed to the flow-tumbling nematic, where $\alpha_3 > 0$ (see the end of § 5 for a short discussion on the backflow effect in flow-tumbling nematics). The stationary solution of (17) gives

$$|\varphi_0| \ll 1 \tag{18}$$

since $\gamma_2/\gamma_1 \approx -1$. The director is thus rotated towards the velocity direction. The solution with $\varphi_0 > 0$ is stable, whereas that with $\varphi_0 < 0$ is not. For MBBA the alignment angle is approximately $\varphi_0 \approx 7°$. Note that when out of equilibrium, the director is rotated anticlockwise only for $|\varphi| < |\varphi_0|$, whereas for any other orientation the stationary state is approached by a clockwise rotation (for the situation as depicted in figure 2).

5. Results and interpretation

5.1. *Field-off relaxation*

In this example the sample is initially aligned in a magnetic field. The field is then switched off instantaneously, and the system relaxes back to the undeformed configuration. In the square cell, the early stages of this relaxation show an anticlockwise central vortex, accompanied by two clockwise eddies at the bottom and top, whereas there are no eddies near the vertical boundaries, figure 3 (*a*). Equations (15) and (16) can explain this asymmetry, for both force contributions depend on the relative orientation of the director with respect to $\nabla\omega$ and $\nabla\varphi$, respectively, which is different for the horizontal as it is for the vertical boundaries. The size of the eddies is of the order of the magnetic coherence length. Their centres are located near the region in which the director field curvature is a maximum ($\varphi = \pi/4$). In the course of time, the maximum curvature region moves to the middle of the cell, and so do the clockwise eddies, figure 3 (*b*). Finally, the central anticlockwise current is completely eliminated. Figure 4 shows the total deformation of the fluid due to the backflow after the relaxation process has stopped.

Let us now take a qualitative look at the forces near the boundaries, considering regions in the middle of the edges where lateral derivatives can be neglected to a first approximation. Only the components parallel to

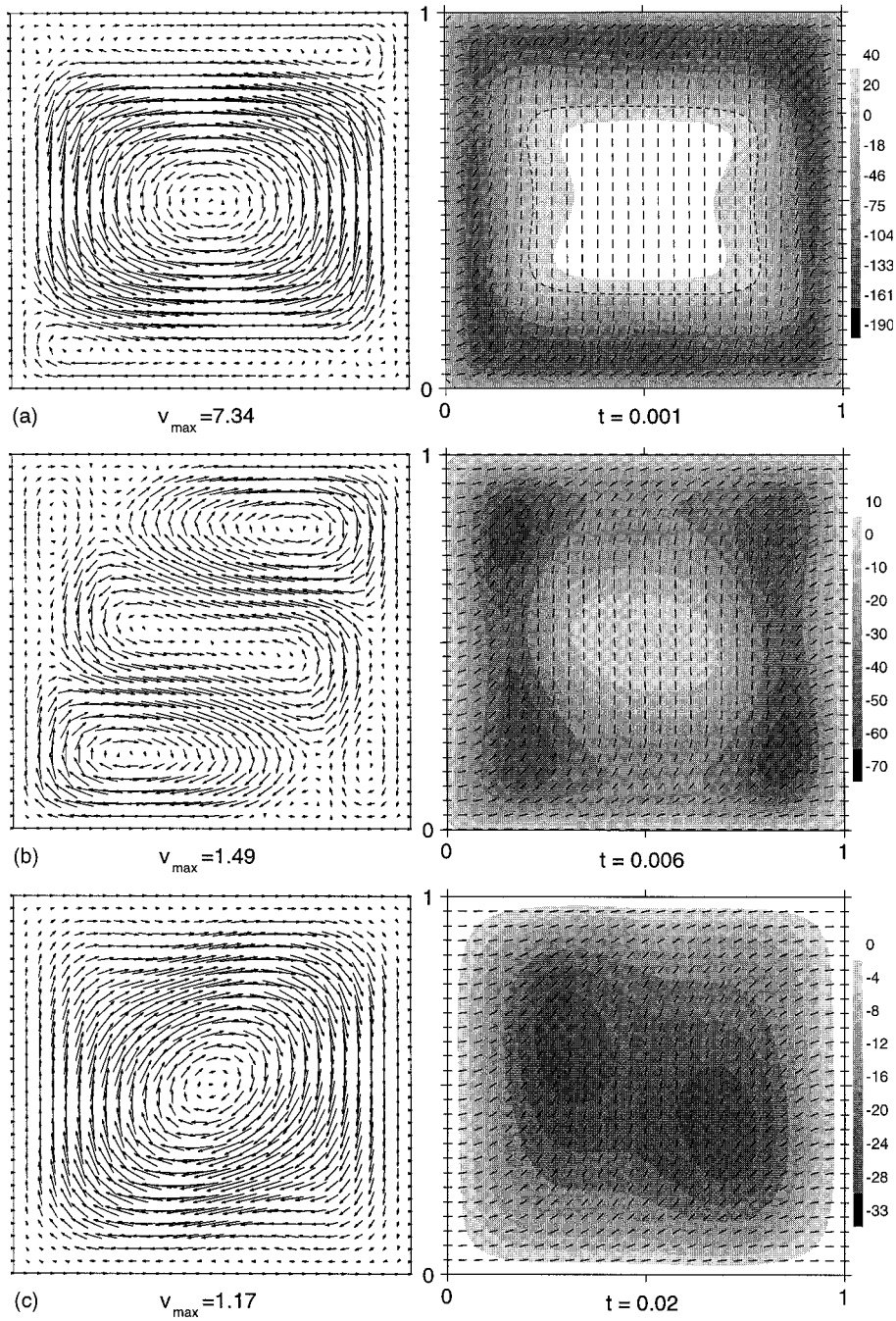

Figure 3. Field off in the square cell: subsequent snapshots of the velocity fields (left column), director fields and director angular velocity fields (represented by levels of gray) show a typical two-step relaxation. (*a*) In the beginning, three vortices are present, while the director in the middle rotates in the opposite sense; the line of the stationary director field is indicated by the dashed contour. (*b*) Clockwise vortices are becoming dominant, note the reverse director deformation at the centre. (*c*) The clockwise vortices have joined to form a single vortex, the sense of rotation now being opposite to that at the beginning. The interior starts rotating in the right sense at a high rate—compare with the rotation in (*a*).

the boundaries are considered, since this must be the direction of the velocity there. One has to realize that the initial relaxation rate $|\omega|$ has a maximum at $\varphi = \pi/4$, since the magnetic force is the strongest there, implying a maximum elastic force to be balanced with. Note that ω is negative. For the outermost parts of the sample, where $\varphi < \pi/4$, $|\omega|$ increases on moving away from the boundary. Hence, equation (15) gives forces trying to start a clockwise current round the cell. However, the forces described by equation (16) oppose the first ones for

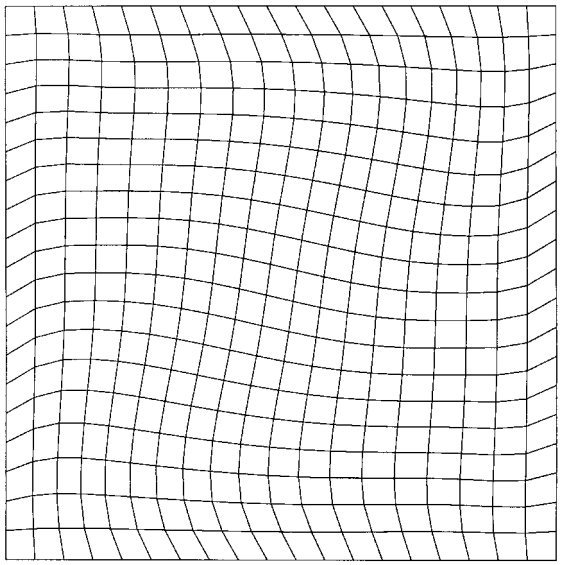

Figure 4. The total deformation of the fluid after the field-off relaxation in the square cell. In the field-on case, the deformation is similar but opposite. Characteristically, to a first approximation it does not depend on the field strength since the backflow velocity scales as $\mathbf{B}^2$, whereas the relaxation time is proportional to $1/\mathbf{B}^2$.

the vertical boundaries, whereas those for the horizontal boundaries add constructively. This is one of the reasons for the missing eddies near the vertical boundaries. Moving further away from the boundaries, φ becomes essentially $\pi/2$ and there are no forces parallel to the boundaries given by equation (16). On the other hand, equation (15) does yield forces for the horizontal boundaries (and none for the vertical ones), starting an anticlockwise current.

Of course, the situation is too complex for the square-shaped cell to be interpreted completely due to the fact that the corners play an important role, the problem there being fully two-dimensional. Therefore we aim to make a more exact analysis for one-dimensional cases, obtained by extending either the horizontal or the vertical boundaries to infinity. In this way, we arrive at the systems studied by Pieranski and co-workers [5, 6] in the limit of weak deformations. Figure 5 (and figure 10 in next section) representing a cell with a 5:1 side ratio, should serve as an illustration for the one-dimensional cases.

Calculations for $L_x \gg L_y$ clearly give three vortices, figure 5 (*a*), whereas those for $L_y \gg L_x$ result in a single vortex only (L_x and L_y are the dimensions of the cell in the x and y directions, respectively). Being able to explain this on the basis of equations (15) and (16) would yield evidence for the non-trivial flow fields being a consequence of the α_2 term in (7). In a one-constant approximation [14, p. 104],

$$h^{\mathrm{em}} = \nabla^2\varphi + \frac{1}{2}B^2 \sin 2\varphi \tag{19}$$

the initial director configuration for large enough fields is

$$\varphi = 2\arctan(\exp(Br)) - \frac{\pi}{2} \tag{20}$$

where $\mathbf{B}$ is the magnetic field used to align the sample (always lying in the vertical direction), and r is the distance from the boundary. This solution is obtained by using the boundary condition $\varphi' = 0$ for $\varphi = \pi/2$, where the prime denotes differentiation with respect to r. The correct condition requires $\varphi' = 0$ for $r = 1/2$ (centre of the cell), which however involves elliptic integrals. Thus, solution (20) is valid if the field is large enough such that for $r = 1/2$ the director is well aligned ($\varphi \approx \pi/2$).

Putting $\omega = \varphi''$ and $\omega' = \varphi'''$, with φ given by the solution (20), one obtains the forces (15) and (16). The components parallel to the boundary are shown in figure 6. They behave as expected from the preceding discussion.

Now let us calculate the approximate initial velocity profiles for both the horizontal and vertical one-dimensional cell. In one dimension, the pressure term and the elastic stress term in equation (14) can be neglected since they can only yield transverse forces (even in more dimensions they are of minor importance, provided that $\nabla \mathbf{v} = 0$ is satisfied). The remaining equation

$$\nabla \sigma^{\mathrm{v}} = 0 \tag{21}$$

is easily solved retaining only the α_2 and α_4 terms in σ^{v}, equation (7). Together with equation (20) the solution reads

$$v(r) = -B^2\frac{\alpha_2}{\alpha_4}\left[\begin{Bmatrix}-\frac{3}{2}\\-\frac{1}{2}\end{Bmatrix}\cos\varphi \pm \frac{1}{6}\cos 3\varphi + C\ln(\cos^{-1}\varphi + \tan\varphi) + D\right]$$

with the constants

$$C = \frac{1}{\ln(\cos^{-1}\varphi_0 + \tan\varphi_0)} \times\left[\begin{Bmatrix}\frac{3}{2}\\\frac{1}{2}\end{Bmatrix}\cos\varphi_0 \pm \frac{1}{6}\cos 3\varphi_0 - \begin{Bmatrix}\frac{4}{3}\\\frac{2}{3}\end{Bmatrix}\right]$$

$$D = \begin{Bmatrix}\frac{4}{3}\\\frac{2}{3}\end{Bmatrix}$$

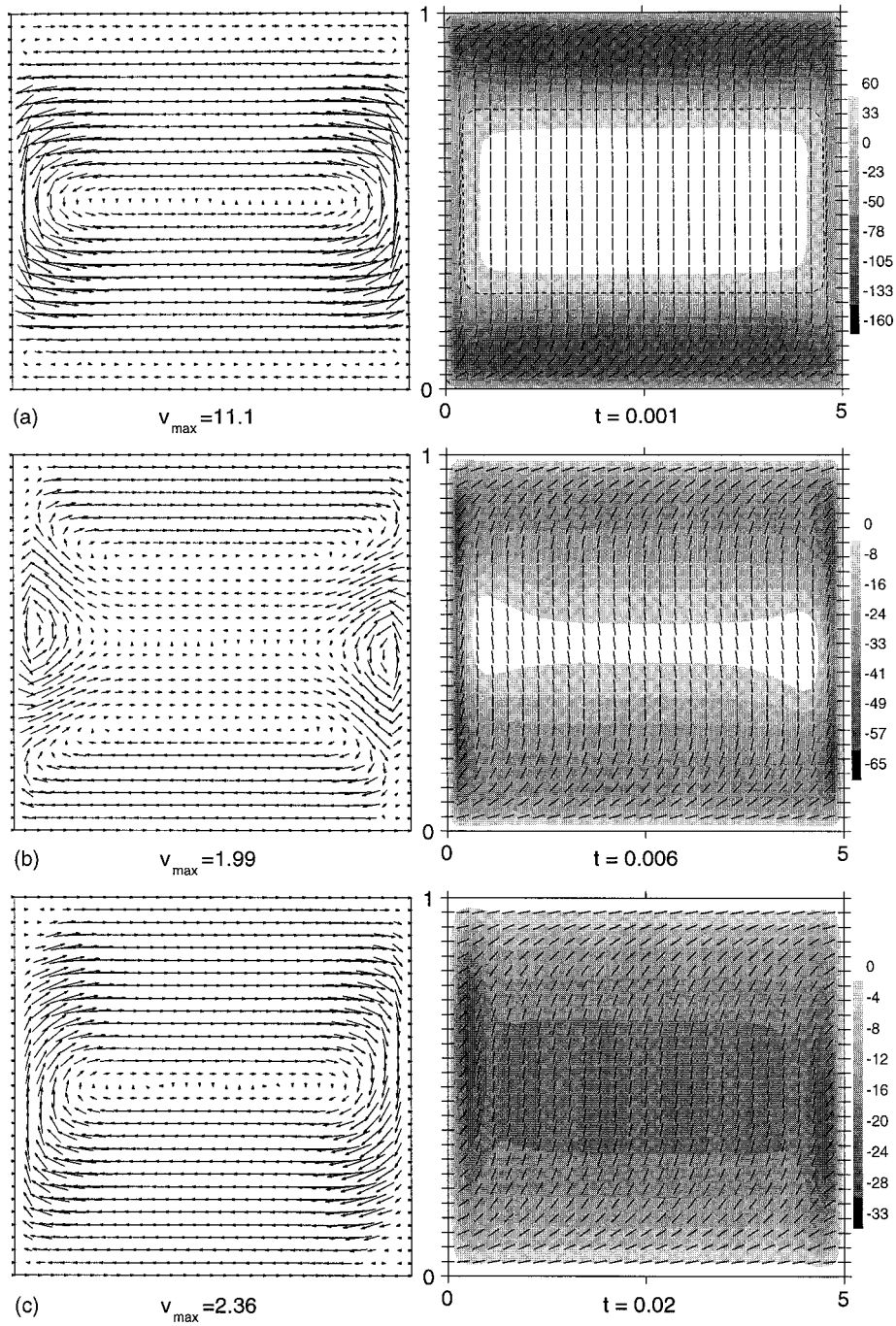

Figure 5. Field off in a horizontal cell with $L_x/L_y = 5$ (note the scale): two-step relaxation. See figure 3 for the key to the figures. (*a*) In the beginning three vortices are formed (figure 7), the director field undergoes a reverse rotation in the middle (note the zero rotation contour, shown dashed). (*b*) At the moment of flow reversal, note the deformation of the central director field. (*c*) A clockwise current results, while the director in the centre is rotating in the right sense at a maximum rate—compare with the rotation in (*a*).

where φ_0 represents the director angle in the middle of the cell. The upper expressions stand for the horizontal cell, the lower ones for the vertical cell. The solutions are plotted in figure 7, and the difference between the horizontal and vertical cases is clearly seen. It is worth pointing out again that, qualitatively, it is also possible to use these results for the regions close to the middle of the boundaries of the square cell, where the situation resembles the one-dimensional case—compare figures 3 (*a*) and 5 (*a*).

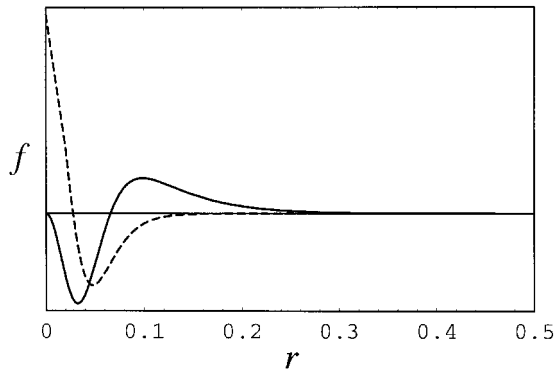

Figure 6. Total initial forces—sum of expressions (15) and (16)—for the horizontal and vertical (dashed) cell as functions of the distance from the boundary ($r = 0.5$ in the centre).

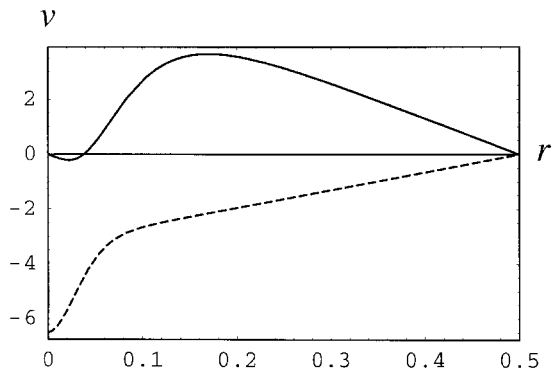

Figure 7. Initial velocity profile, equation (21), for the horizontal and vertical (dashed) cell ($\mathbf{B} = 20$). In the horizontal case, two opposing currents are predicted. The width of the counter-current near the boundary is of the order of the magnetic coherence length. On the other hand, the vertical cell gives a single current only, although the net force changes sign near the boundary (figure 6). Both analytical predictions based on the simplified viscous stress tensor are consistent with numerical results.

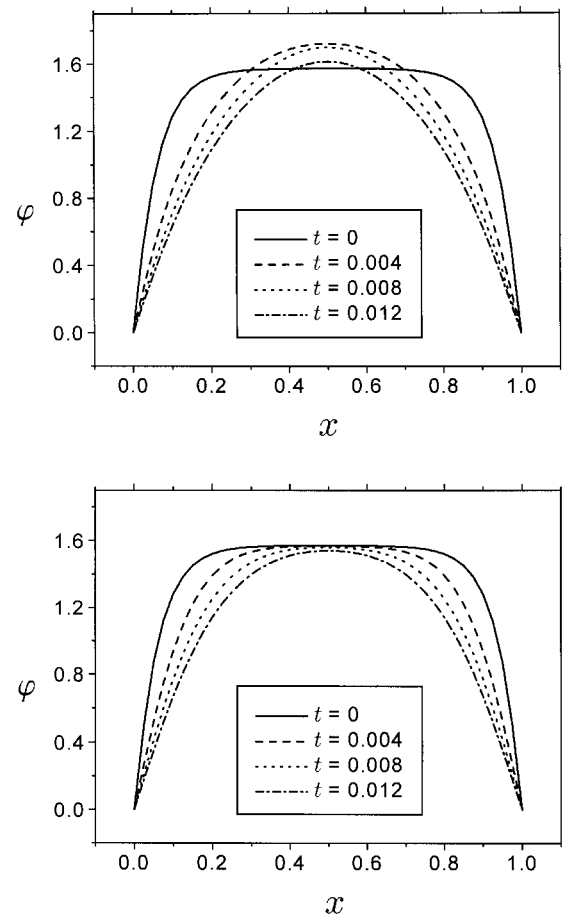

Figure 8. Vertical cross-sections through the centre of the horizontal cell (field-off): director angle as a function of transverse coordinate is shown for subsequent moments in time (early stage only). The backflow alters the process in the centre (above), compared with the simple relaxation without the flow (below).

So far, only the generation of the backflow has been studied. We now consider the inverse phenomena of how the backflow influences the director rotation. In both one-dimensional cases we are confronted with pure shear flow, the effect of which are described by equation (17). The situation is now completely different for the horizontal and vertical cases. In the horizontal case, the shearing backflow slows the director rotation in the middle of the cell, figure 5(*a*), and is moreover actually able to reverse the direction of rotation due to the weak elastic forces there, figures 5(*b*) and (8). This phenomenon is known as the *kickback* effect [17, p. 167]. Near the boundaries, however, the shear is opposite, thus accelerating the relaxation. As a result, the gradient of ω becomes larger, which induces an even stronger backflow (a positive feedback effect). One has to keep in mind that the backflow effect is only a perturbation to the relaxation which, in this case, is governed by elastic forces. Thus, when talking about the positive feedback, one must remember that this is only a small contribution to the director and flow fields, whereas global behaviour is still set by the elasticity. Eventually, elastic forces become dominant even in the middle of the cell (figure 8), reversing the rotation of the inner part and accelerating it, while slowing the rotation of the outer part. We are then left with the centre reorienting faster than the edges, figures 5(*c*) and 8, a situation opposite to the initial one. As a result, the backflow also changes direction, transforming from an anticlockwise central current with two opposite eddies at the top and bottom to a single clockwise current. The latter is then stable; accelerating the relaxation in the middle of the cell it grows stronger initially (a positive feedback again), then slowly fades as the elastic forces vanish. This type of process where, in a region of the sample, the director is rotated backwards for some period

of time and then the flow direction is suddenly reversed, will be referred to as a two-step relaxation. One can notice that in the square cell the relaxation path is quite similar. The kickback effect is observed, figures 3(*a*) and 3(*b*), as well as the reversal of the flow, figure 3(*c*).

For the vertical case, however, in the middle of the cell the director is not rotated backwards by the backflow, but merely held in the field-aligned orientation. By contrast, near the boundaries the reorientation is accelerated by the backflow as for the horizontal case. As a result, the relaxation proceeds from the edges and then gradually bites to the centre, much like the case of a simple relaxation without taking into account the backflow (figure 8, lower diagram). This conserves the direction of the current. One can call a process like this a one-step relaxation. Eventually, we end up with a reverse current in this case also, but this happens much later and when the sample has almost relaxed. Also, the reversal of the current proceeds very slowly and steadily from the outside; it does not happen suddenly in the whole cell as in the horizontal case.

5.2. *Field-on relaxation*

Now we consider the case in which the initial director field is undeformed, and a vertical magnetic field is applied at a small angle (2°) off the normal to the director, which does not significantly alter the critical behaviour of the transition [17, p. 105]. Due to the increasing rate of rotation ω toward the centre, an anticlockwise current is predicted by equation (15), while the force (16) is initally unimportant, since the director is uniform. Calculations for the square cell show that in the course of time the current is split into two vortices, while in between these two clockwise vortices are also formed, and we finish with 4 major vortices, figure 9(*b*).

Again it is useful if one first focuses on the one-dimensional cases. For the horizontal cell initially there is no current, because the director is perpendicular to the gradient of ω, equation (15). If the cell is not infinite, but just extended in the horizontal direction, the flow is limited to the short boundaries, where $\nabla\omega$ points along the director. For a long cell, however, this is unimportant. When the director turns a little, the force (15) becomes larger initiating the anticlockwise current. With the deformed director field the force (16) also starts contributing to the anticlockwise current. After the director has reached the angle of instability (18) in the centre, the reorientation is accelerated by the current, resulting in a positive feedback strengthening the backflow. The positive feedback is greatly amplified by the magnetic torque, which in this case is the driving force of the relaxation. It acts like a fuse triggering the magnetic torque by rotating the director off the field normal, equation (19). On the other hand, near the boundaries the relaxation is slowed by the shear there having opposite sign (the director tends to stay flow-aligned). Consequently, when eventually the relaxation ceases in the middle of the cell, the outer parts are still relaxing. Now the force (15) changes direction, trying to start a clockwise current. It is opposed by the $\nabla\varphi$ dependent force (16), which is strongest near the boundaries. As a result, the flow dies out in the middle of the cell first, followed by a cessation at the boundaries.

Again the situation is quite different for the vertical case (figure 10). However, unlike the field-off relaxation, now it will be the more interesting one. Here the anticlockwise flow due to the force (15) is initiated immediately, since now $\nabla\omega$ points along the director. Moreover, in the middle of the cell the shear starts to rotate the director at a maximum rate as a result of being normal to the director, equation (17). On the other hand, near the boundaries the shear is opposite, thus turning the director in the reverse sense, again at a maximum rate, figure 10(*a*). Here we are dealing with two effective mechanisms that turn on the magnetic torque, one in the middle of the cell generating an accelerated anticlockwise rotation, the other at the boundaries causing clockwise rotation, which is also amplified by the magnetic field. Hence, this gives rise to a strong anticlockwise current first (positive feedback again), as confirmed by figure 10(*a*). However, the force (16), becoming more important as the deformation increases, opposes the clockwise rotation. The flow is thus subject to a kind of frustration. As a result of this, it is able to change direction very rapidly, as the force (15) ceases. One can make an estimation of the director angle at which the net force changes sign, using $\omega = 1/2B^2 \sin 2\varphi$ with equations (15) and (16), yielding

$$f = \frac{1}{2}\alpha_2 B^2 (2\cos^2 2\varphi + \cos 2\varphi - 1)\varphi'.$$

This gives $\varphi = 30°$ for the angle of force reversal. Since the angle is maximum in the centre of the sample, this is where the flow reversal is initiated. After some time, the interior has almost relaxed when the outer director field just begins to rotate in the right sense, figure 10(*b*). The gradient of ω is reversed, the force (15) changes direction, now acting in accordance with the force (16). The clockwise current accelerates the relaxation of the outer part (positive feedback) while additionally slowing the rotation in the centre, figure 10(*c*). Interestingly, this current is larger than the initial anticlockwise current.

Thus, for the field-on relaxation, the interesting scenario also involves two steps: in the beginning a weak magnetic torque generates backflow due to non-uniform rotation. In some regions, the backflow accelerates the

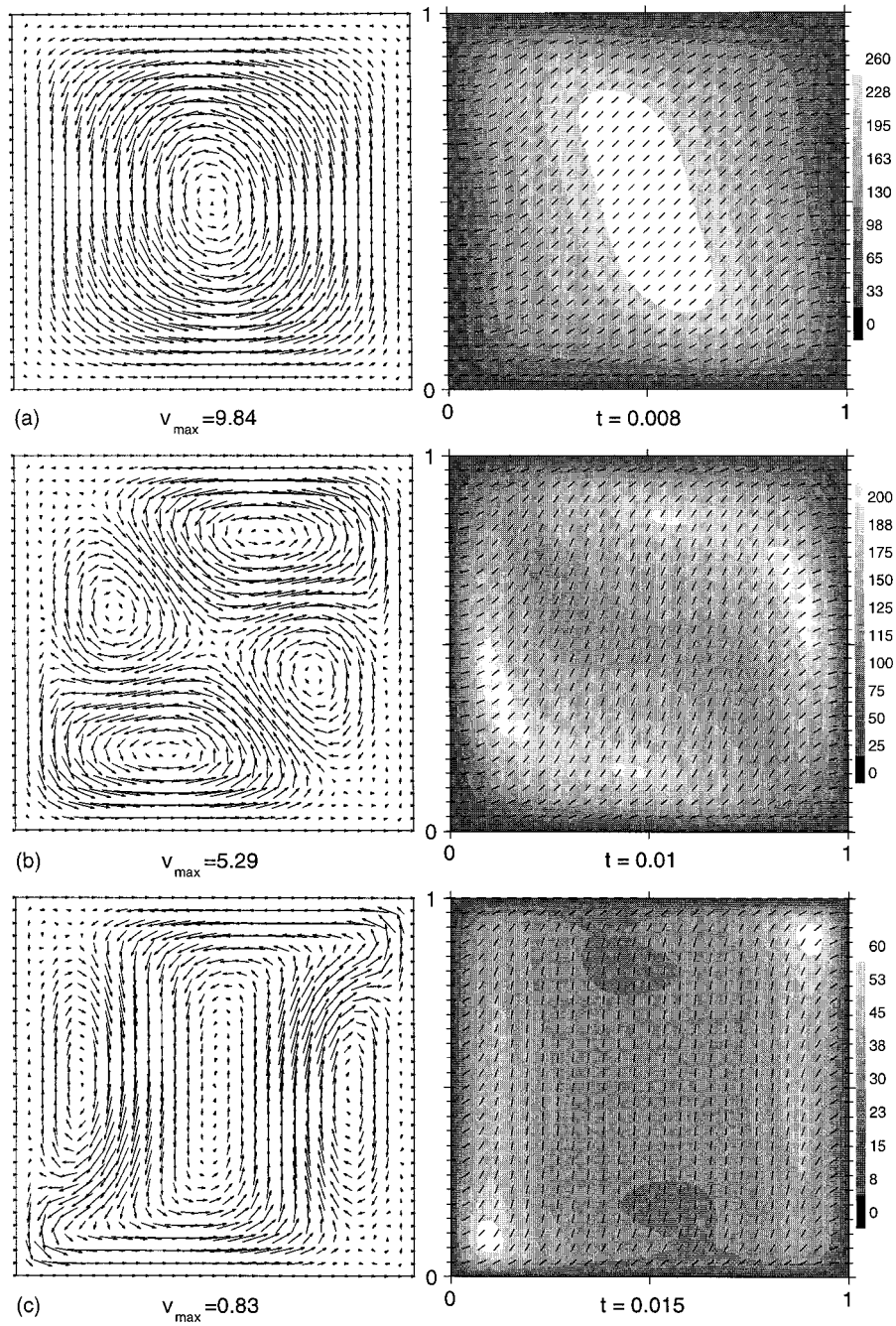

Figure 9. Field on in the square cell: see figure 3 for the key to the figures. (*a*) The director rotation is maximum in the middle; the asymmetry of the corners is due to the backflow, not to the differences in the splay and bend elastic constants. (*b*) Now the centre is relaxing slower, as are the NW and SE corners, which were faster in (*a*); an interesting four-fold flow pattern is observed. (*c*) Late stages of relaxation; the current has not changed direction completely.

rotation which has a major effect because in this way the magnetic torque becomes progressively larger and larger. Consequently, these regions are relaxed much more quickly than those for which the backflow has a retarding effect. As a result, they are already far above the angle of maximum magnetic torque when the delayed regions arrive at it. Now the latter regions relax faster, which causes the backflow also to change direction. The two-step scenario is fully developed in the vertical case, whereas the horizontal cell relaxes more or less in one step, as described previously.

The sudden formation of four vortices in the square cell can also be explained by this mechanism, only that now all four boundaries are important, resulting in a

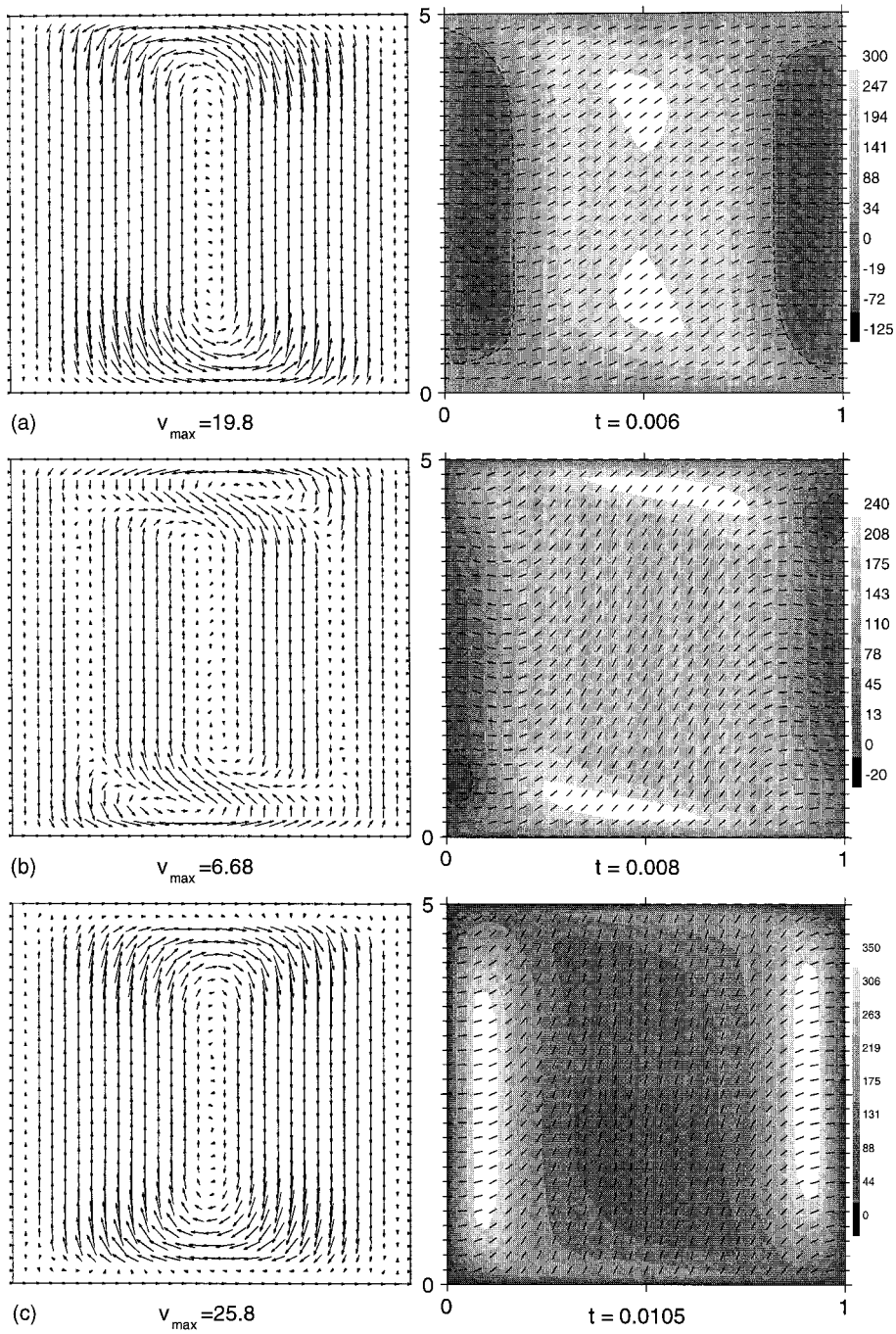

Figure 10. Field on in the vertical cell with $L_y/L_x = 5$ (note the scale), two-step relaxation: see figure 3 for the key to the figures. (*a*) Flow-induced backward rotation near the vertical boundaries is amplified by the field (contour of zero rotation is shown dashed). (*b*) Backflow is changing direction, note the director deformation near the vertical boundaries. (*c*) The flow has changed direction, as well as the gradient of ϕ. The situation is similar to that in (*a*), but reversed; note that the velocities are large in magnitude.

more complex fourfold low pattern figure 9 (*b*). Clearly the flow reversal mechanism is present in this case also, yet towards the end the original flow direction is restored. However, calculations for $L_y/L_x = 2$ already yield a definite flow reversal.

Finally, it should be mentioned that the processes studied in this paper do not depend critically on the sign of the Leslie coefficient α_3, which sets the flow-aligning or flow-tumbling properties of the nematic, subject to the simple shear flow. If α_3 is set to zero or

even its sign is reversed (keeping its value small), no radical changes are observed. For our discussion to be valid, only the condition $|\alpha_3/\alpha_2| \ll 1$ must be satisfied.

6. Comparison with the simplified treatment

The relaxation with the backflow is to be compared now with the simplified relaxation without taking into account the backflow. Figure 11 shows the time dependence of $\sin^2\varphi$, averaged over the square cell, for both the full and simple treatments. Here the effect of the backflow is mainly to speed-up the relaxation process, a situation that is most frequently observed. In some cases, however, the influence of the backflow is more complicated and one cannot speak simply about changes of the relaxation rate. This occurs in the vertical cell if a strong enough field is applied so that the two-step process becomes very distinct (figure 12). At a lower field strength, on the other hand, the simple regime is again restorted (figure 13).

The importance of the geometry is clearly seen if one compares figures 12 and 14, showing the time dependences of the Fourier components of $\sin^2\varphi$ in the vertical and the horizontal cells, respectively. The fields are rescaled relative to the critical field

$$B_c^2 = \frac{K_{33}}{K_{11}}(\pi/L_x)^2 + (\pi/L_y)^2 \qquad (22)$$

so that the ratio B/B_c is the same in both cases, allowing one to make a direct comparison. Evidently, when turning on the field, the backflow effect is much stronger in the vertical cell (two-step process) than in the horizontal cell (single-step process). As far as the field-off relaxation is concerned, the same conclusion holds. There the effect is stronger in the horizontal geometry, which in this case yields the two-step scenario.

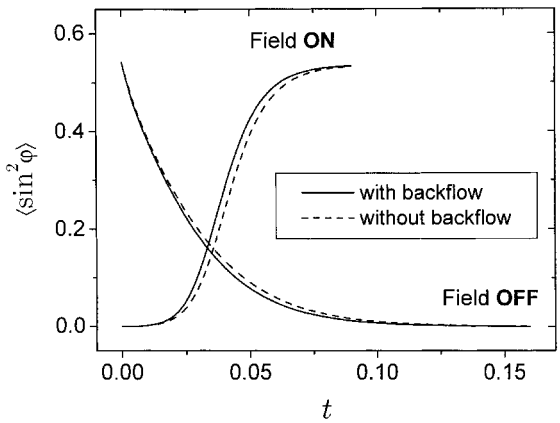

Figure 11. Time dependence of $\sin^2\varphi$ (square cell), averaged over the cell, for cases with and without taking into account the backflow. Magnetic field of strength $B = 10$ is turned on and off.

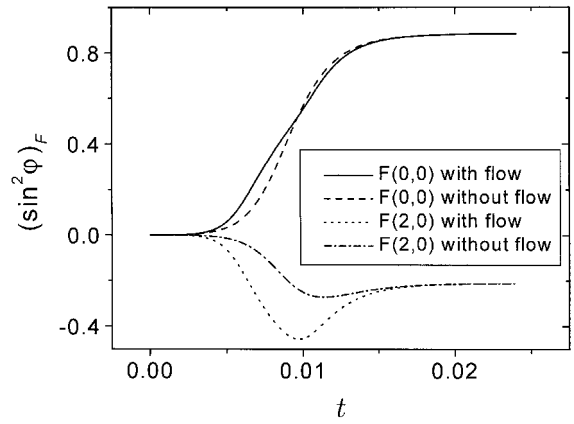

Figure 12. Time dependence of the largest cosine Fourier components of $\sin^2\varphi$, for the full and the simplified treatment (vertical cell, magnetic field of strength $B = 20$ is turned on). The average is denoted by $F(0, 0)$, whereas $F(2, 0)$ stands for the component belonging to $\cos(2\pi x/L_x)$. It is shown that the average behaviour can be more complicated than normal (compare figures 11 or 14). Note that the difference is much larger for the $F(2, 0)$ components than for the averages, indicating that due to the backflow the rotation is indeed faster in the middle of the cell and slower near the boundaries (see also figure 10).

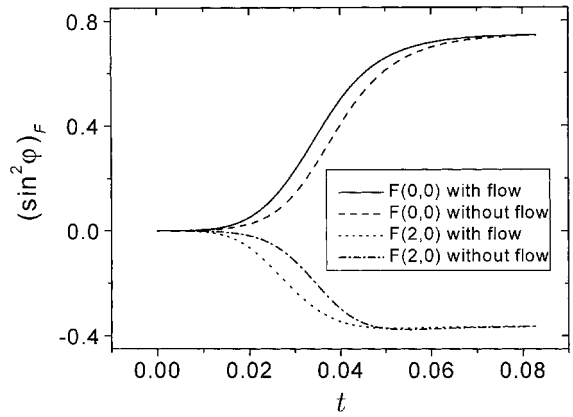

Figure 13. Time dependence of the cosine Fourier components of $\sin^2\varphi$, defined in figure 12, for the full and simplified treatments (horizontal cell, magnetic field of strength $B = 10$ is turned on). Note that due to the weaker field the average behaviour is less complex, when compared with figure 12.

7. Conclusion

In this paper, two-dimensional nematodynamic problems have been studied in their full form, making no approximation other than a low Reynolds number, which is practically exact for the problems concerned. First, one must note the remarkable non-triviality of the generated velocity fields, i.e. the formation of several vortices, despite the simple geometry and strictly laminar flow. This is a consequence of the delicate interconnections between the director and the flow field. In

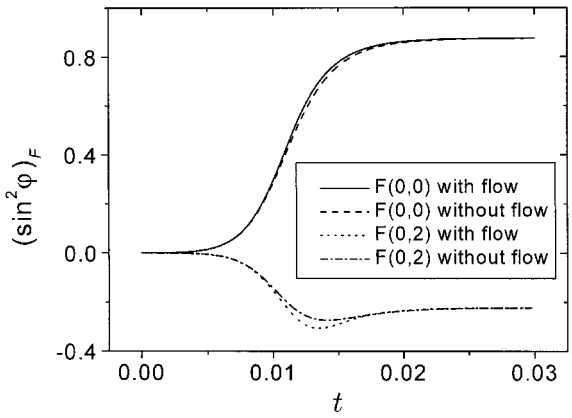

Figure 14. Time dependence of the cosine Fourier components of $\sin^2\varphi$, defined in figure 12, for the full and simplified treatments (horizontal cell, magnetic field of strength $B = 20$ is turned on). The figure should serve as a contrast to figure 12, showing that the backflow effect is less pronounced in the horizontal cell.

addition, it has been shown that the form of the backflow, as well as its time evolution, depend very much on the geometry of the system, as does the influence of the backflow on the director reorientation. It is stronger for the two-step processes, which are characterized by a global reversal of the flow direction.

Besides numerical solutions, this paper also highlights the qualitative picture of the backflow problem. Thus, following the discussion of § 5, one is able to foresee the global flow dynamics in the cell, without having to perform any extensive numerical calculations. In particular, it is worth pointing out again that the backflow scenario depends crucially on the relative orientation of the magnetic field with respect to the long axis of the cell. It has been assumed that $|\alpha_3/\alpha_2| \ll 1$ holds for the two Leslie coefficients, whereas the sign of α_3 has proved not to be significant.

From the experimental viewpoint, the results presented in this paper are directly applicable to samples confined in tubes of square or rectangular cross section. In this case, the geometry is essentially two-dimensional, while additionally the in-plane magnetic field constrains the director to the planar orientation. The switching of pixels in a classic nematic display is a more useful example. A pixel is a part of a liquid crystal cell that is controlled by a local electric field. This system is relatively close to the cases of elongated cells presented in this paper. Usually, the pixel is thin compared with its lateral size. However, if the director rotates in a plane normal to the pixel plane, one can, as a reasonable approximation, make use of our results for the rectangular-shaped cells. Thus, in this case the geometry of the calculation is defined by the cross-section of the switching plane with the pixel. The dimensions of the rectangle so obtained are the pixel thickness and its lateral size. Despite the fact that only cells with a 5 : 1 side ratio were presented in this paper, ratios of 20 : 1 or more can be reached on a regular basis.

Our results can also be used in the case of in-plane switching pixels, where the director rotation takes place in the pixel plane. However, the extent of agreement would strongly depend on the boundary conditions at the upper and lower pixel plane. If the rotation of the director is not hindered too much at the boundaries and the no-slip boundary condition for the velocity is not strictly satisfied then the agreement with our calculation should be good.

The effect of finite anchoring strengths has not been studied. Nevertheless, one can state that for decreasing anchoring strength the backflow velocity, and thus the torque exerted on the director, start decaying as $1 - \xi/\xi_m$, where ξ and ξ_m are the extrapolation and the magnetic coherence length, respectively. This means that the anchoring strength should be kept strong ($\xi/\xi_m \ll 1$) in order to observe any backflow effects.

If one wanted to consider the experimental or application situation more closely, a full three-dimensional calculation would be needed. With this, however, the treatment would become numerically quite demanding. It is also doubtful whether a complete solution to the problem would bring much benefit, since the effect of the backflow is limited more or less to quantitative corrections, as demonstrated in this paper. Nevertheless, there are special cases where the backflow plays a decisive role and crucially alters the evolution path of the system. For example, the amplification of the kickback effect (see § 5.1) by a horizontal magnetic field leads to the creation of a domain wall. This phenomenon would never take place if the backflow was not present.

Besides specific examples of this kind, there is another type of problem where the backflow is expected to be very important, namely the relaxation of structures containing defects, for example attraction of defects, defect annihilation, and so on. The introduction of defects to the director field, however, brings about enormous technical difficulties considering the discretization, this having prevented these problems from being solved for several years although sufficient computer power has been available. Therefore, our future research will be aimed at examining these areas.

This work was supported by the Ministry of Science and Technology of Slovenia (Grant No. J1-0595-1554-98), US-Slovene NSF Joint Found (Grant No. 9815313), and SILC TMR ERBFMRX-CT98-0209 project. The authors are grateful to Prof. A. Kodre and Prof. G. Durand for fruitful discussions and the interest they have shown in the subject.

References

[1] Ericksen, J. L., 1960, *Arch. ration. Mech. Analysis*, **4,** 231.
[2] Leslie, F. M., 1966, *Quart. J. Mech. appl. Math.*, **19,** 357; Leslie, F. M., 1968, *Arch. ration. Mech. Analysis*, **28,** 265.
[3] Clark, M. G., and Leslie, F. M., 1978, *Proc. r. Soc. Lond. A*, **361,** 463.
[4] Van Doorn, C. Z., 1975, *J. Physique*, **36,** C1-261.
[5] Brochard, F., Pieranski, P., and Guyon, E., 1972, *Phys. Rev. Lett.*, **26,** 1681.
[6] Pieranski, P., Brochard, F., and Guyon, E., 1973, *J. Physique*, **34,** 35.
[7] Carr, E. F., 1977, *Mol. Cryst. liq. Cryst.*, **34,** 159.
[8] Guyon, E., Meyer, R., and Salan, J., 1979, *Mol. Cryst. liq. Cryst.*, **54,** 261.
[9] Hurd, A. J., Fraden, S., Lonberg, F., and Meyer, R. B., 1985, *J. Physique*, **46,** 905.
[10] Migler, K., and Meyer, R., 1991, *Phys. Rev. Lett.*, **66,** 1485.
[11] Migler, K., and Meyer, R., 1993, *Phys. Rev. E*, **48,** 1218.
[12] Bajc, J., Hillig, G., and Saupe, A., 1997, *J. chem. Phys.*, **106,** 7372.
[13] Polimeno, A., and Martins, A. F., 1998, *Liq. Cryst.*, **25,** 545.
[14] De Gennes, P. G., and Prost, J., 1995, *The Physics of Liquid Crystals* (Oxford: Clarendon Press).
[15] Vertogen, G., and de Jeu, W. H., 1998, *Thermotropic Liquid Crystals, Fundamentals* (Berlin: Springer-Verlag).
[16] Fletcher, C. A. J., 1988, *Computational Techniques for Fluid Dynamics*, Vol. II (Berlin: Springer-Verlag).
[17] Chandrasekhar, S., 1992, *Liquid Crystals* (Cambridge: Cambridge University Press).